

Structure–Activity Relationship Studies of Indole-Based Compounds as Small Molecule HIV-1 Fusion Inhibitors Targeting Glycoprotein 41

Guangyan Zhou,[†] Vladimir Sofiyev,[†] Hardeep Kaur,[†] Beth A. Snyder,[§] Marie K. Mankowski,[§] Priscilla A. Hogan,[§] Roger G. Ptak,[§] and Miriam Gochin^{*,†,‡}

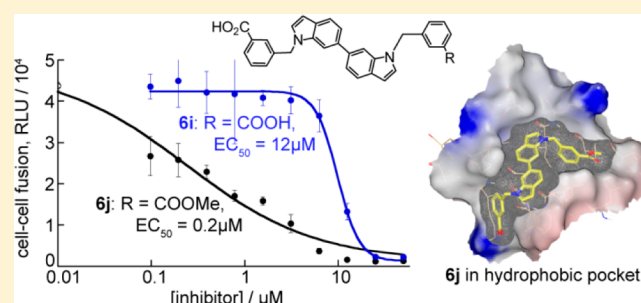
[†]Department of Basic Sciences, Touro University—California, 1310 Club Drive, Mare Island, Vallejo, California 94592, United States

[‡]Department of Pharmaceutical Chemistry, University of California—San Francisco, San Francisco, California 94143, United States

[§]Southern Research Institute, 431 Aviation Way, Frederick, Maryland 21701, United States

Supporting Information

ABSTRACT: We previously described indole-containing compounds with the potential to inhibit HIV-1 fusion by targeting the hydrophobic pocket of transmembrane glycoprotein gp41. Here we report optimization and structure–activity relationship studies on the basic scaffold, defining the role of shape, contact surface area, and molecular properties. Thirty new compounds were evaluated in binding, cell–cell fusion, and viral replication assays. Below a 1 μM threshold, correlation between binding and biological activity was diminished, indicating an amphipathic requirement for activity in cells. The most active inhibitor **6j** exhibited 0.6 μM binding affinity and 0.2 μM EC_{50} against cell–cell fusion and live virus replication and was active against T20 resistant strains. Twenty-two compounds with the same connectivity displayed a consensus pose in docking calculations, with rank order matching the biological activity. The work provides insight into requirements for small molecule inhibition of HIV-1 fusion and demonstrates a potent low molecular weight fusion inhibitor.



for some of the small molecules, although they had IC_{50} values of several micromolar against cell–cell fusion.^{18,20} Low molecular weight compounds able to potently inhibit HIV-1 fusion remain elusive, notwithstanding the important role they could play in countering multidrug resistance, viral latency, and the cell-to-cell route of transmission thought to be responsible for rapid spread and resurgence of the virus.²¹ We recently described the development of a series of indole compounds as hydrophobic pocket binding fusion inhibitors.²² Two benzyl-substituted bisindole compounds containing four aromatic ring systems demonstrated $\sim 0.9 \mu\text{M}$ activity against cell–cell and virus–cell fusion (Figure 1). In this work, we have performed lead optimization based on this scaffold, where we describe SAR studies examining isomeric forms, alternative benzyl ring and

INTRODUCTION

Fusion of human immunodeficiency virus type 1 (HIV-1) with host cells is mediated by viral envelope glycoprotein 41 (gp41) through a series of conformational rearrangements culminating in the formation of a six-helix bundle (6-HB) between N-heptad repeat (NHR) and C-heptad repeat (CHR) regions of the extracellular domain of gp41 trimer.^{1–3} Any chemical entity that disrupts 6-HB formation has the potential to inhibit the fusion process, thereby blocking HIV-1 entry into the target cells.⁴ C-peptide inhibitors derived from the CHR have been shown to be potent inhibitors of HIV fusion,⁵ and time of addition experiments have revealed that they typically remain active for 30–90 min after initiation of viral infection.^{1,6} Thus, it appears that a fairly long-lived intermediate conformation of gp41 exists in which the NHR coiled coil in the gp41 trimer is exposed and susceptible to inhibition. Peptides directed against different regions of gp41 have been developed into drugs or drug candidates.^{7–9} They are useful in salvage therapy against HIV strains resistant to HAART therapy or can be used as vaccine antigens¹⁰ or microbicides,¹¹ but suffer from the usual limitations of peptide drugs, including shelf life, stability, bioavailability, and cost.

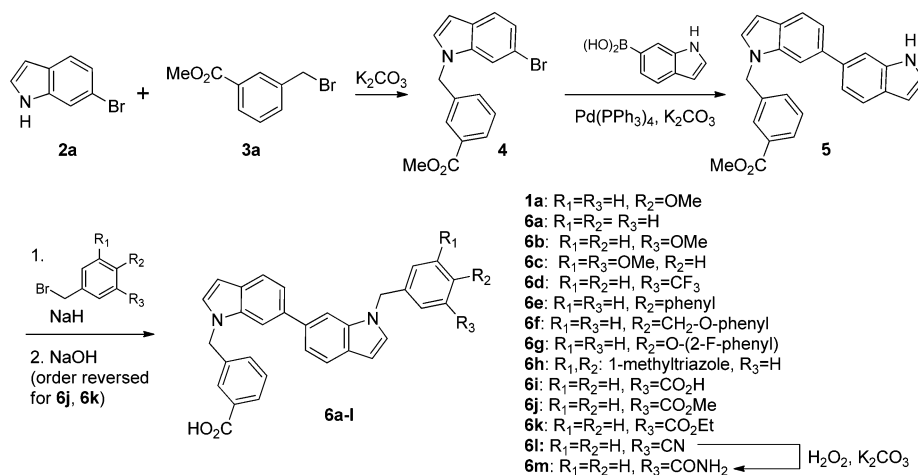
Multiple studies have shown that D-peptides and small molecules targeting a conserved hydrophobic pocket on the coiled coil^{12–14} have fusion inhibitory properties.^{11,15–20} Antiviral activity at low nanomolar concentrations was described

Figure 1. Structure of lead compounds **1a** and **1b**.

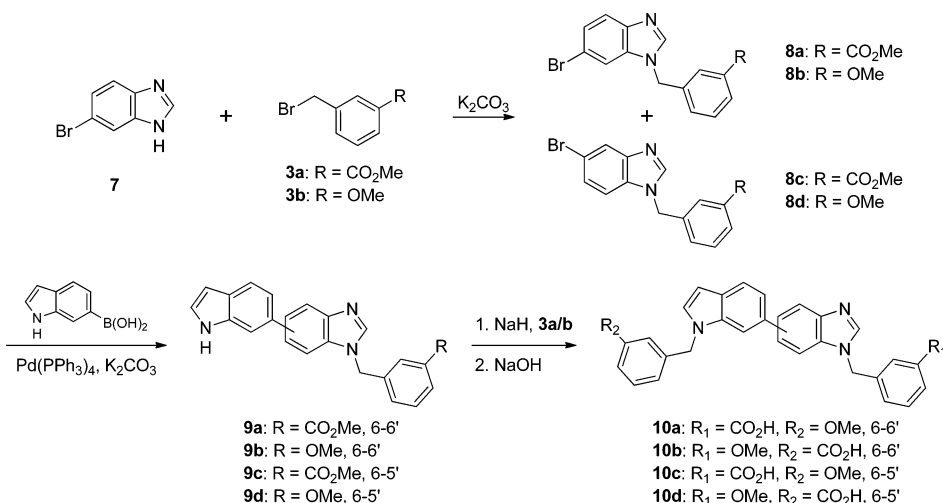
Received: March 4, 2014

Published: May 24, 2014

Scheme 1. Synthesis of Bisindole Compounds



Scheme 2. Synthesis of Benzimidazole-Indoles



other substituents, and compounds containing benzimidazoles. The work has resulted in several 6–6' linked bisindole compounds with submicromolar activity against cell–cell and virus–cell fusion, including **6j** with $\text{EC}_{50} = 200$ nM, and has provided an assessment of molecular properties associated with potency. The two most active compounds **6j** and **6k** were tested and found to be effective against multiple strains of HIV, including a strain that is resistant to T20.²³ These compounds are a promising advancement in fusion inhibitor design.

CHEMISTRY

The synthesis of compounds containing four aromatic systems is described in Schemes 1–3. Derivatives of **1a** with alternative substitutions on ring D were synthesized as shown in Scheme 1 (compounds **6a–m**). The synthesis has been improved since our previous paper,²² taking advantage of the common intermediate **5** that is accessed through Suzuki–Miyaura cross-coupling to form the bisindole scaffold.^{24,25} Alternative linkage through the 5-position of the indole (**6o–q**) was explored using a similar synthetic strategy with 5-bromoindole or indole-5-boronic acid as the starting material (Scheme S1 in Supporting Information). For the benzimidazole series **10a–d** (Scheme 2), alkylation of 6-bromobenzimidazole formed both 5- (**8c** or **8d**) and 6-bromobenzimidazole (**8a** or **8b**) intermediates in one pot. The

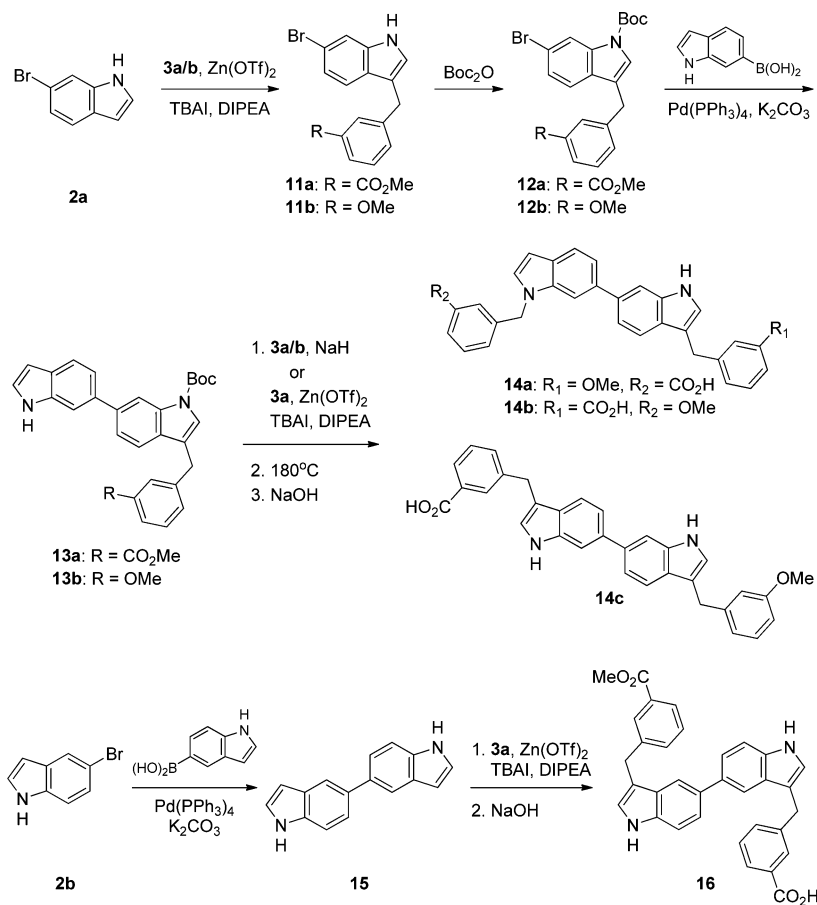
two isomers were separated by flash chromatography, and their structures were verified by ROESY correlations between benzimidazole six-membered ring protons and the methylene of the attached benzyl moiety (Supporting Information Figure S1).

Compounds **14a**, **14b**, **14c**, and **16** were made having one or both indoles substituted at the 3-position (Scheme 3) to take advantage of a potential NH interaction in the hydrophobic pocket. The compounds in this series were prepared using $\text{Zn}(\text{OTf})_2$ mediated alkylation of the 3-position with benzyl bromides.²⁶ All potential combinations were prepared including the 1,3'-, 3,1'-, and 3,3'-substituted bisindoles to complement the previously prepared 1,1'-substituted **6b**. In addition, a 5–5' linked bisindole **16** was made that is 3,3'-substituted and has a complementary shape to **6j**. Truncated compounds with three aromatic ring systems were included in the SAR analysis to gauge the effect of compound size (Scheme 4), some of which were obtained by saponification of corresponding methyl ester intermediates (**18b**, **20a,b**, **23**).

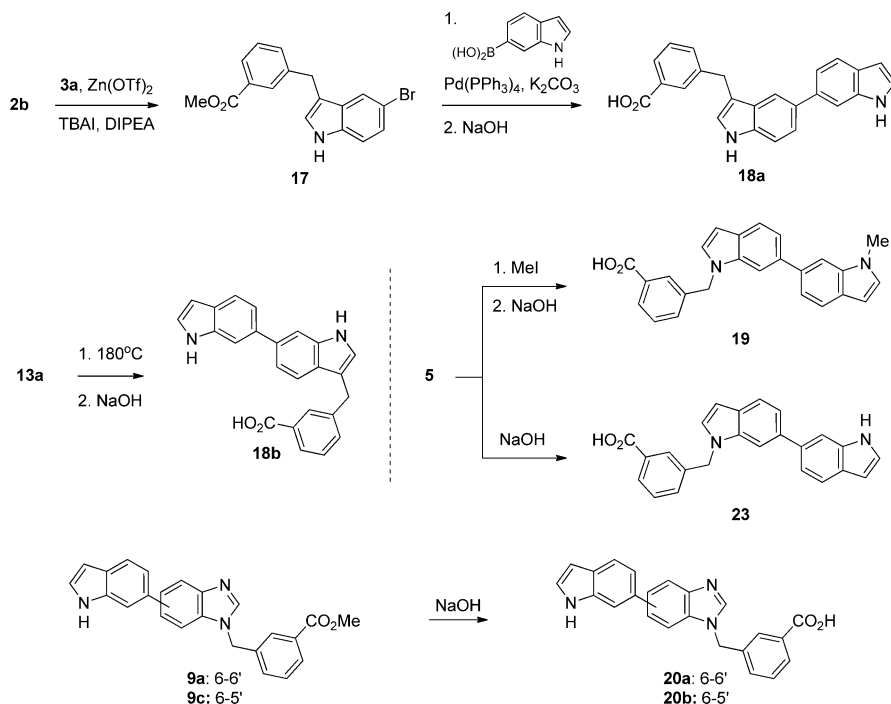
RESULTS AND DISCUSSION

The most active previously synthesized compounds **1a**, **1b**²² with four aromatic systems labeled A–D (Figure 1) had virtually identical binding affinity and in vitro potency. Binding affinity

Scheme 3. Synthesis of 3-Substituted Indoles



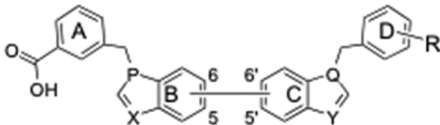
Scheme 4. Synthesis of Truncated Bisindoles



(K_i) to the hydrophobic pocket was on the order of 1–2 μ M and the compounds exhibited comparable activity against cell–cell fusion ($EC_{50}^{CCF} = 0.5$ –1.0 μ M) and viral infectivity ($EC_{50}^{VCF} =$

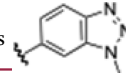
0.9 μ M). The following aromatic system substitutions were made: indole B was replaced with benzimidazole (10a, 10c, 20a, 20b); the benzoic acid substituent was moved to the 3-position

Table 1. Biochemical and Cell-Based Assay Data in μM for Compounds with Four Aromatic Ring Systems



compd	X/P	Y/Q	R	link	K _i ^a	EC ₅₀ fusion inhibition			TC ₅₀ toxicity	
						CCF HXB2 ^b	VCF Ba-L ^c	VCF IIIB ^c	resazurin ^b	MTS ^c
Bis-indole Linkage										
1a	CH/N	CH/N	<i>p</i> -methoxy	6–6′	1.0 ± 0.2	0.8	0.9	0.9	20	32
6o	CH/N	CH/N	<i>p</i> -methoxy	5–6′	3.0 ± 0.4	7	18	19	>100	18
6p	CH/N	CH/N	<i>p</i> -methoxy	6–5′	4.2 ± 0.3	3.5	6.9	8.3	91	24
6q	CH/N	CH/N	<i>p</i> -methoxy	5–5′	3.9 ± 0.4	12	18	20	>100	55
Carboxyl Substituent R										
6i	CH/N	CH/N	<i>m</i> -COOH	6–6′	0.6 ± 0.1	12	58	67	>100	>100
6j	CH/N	CH/N	<i>m</i> -COOMe	6–6′	0.6 ± 0.2	0.2	0.2	0.2	53	15
6k	CH/N	CH/N	<i>m</i> -COOEt	6–6′	1.0 ± 0.2	0.7	0.3	0.5	>50	43
6m	CH/N	CH/N	<i>m</i> -CONH ₂	6–6′	0.8 ± 0.2	6	39	51	>100	>100
6n	CH/N	CH/N	<i>m</i> -COOH	6–5′	0.7 ± 0.1	2	20	17	>100	>100
Nonpolar Substituent R										
1b	CH/N	CH/N	<i>p</i> -F	6–6′	1.7 ± 0.3	1.1	1.6	nd	>25	52
6a	CH/N	CH/N	H	6–6′	3.5 ± 1.3	2	4.4	4.6	>50	>100
6b	CH/N	CH/N	<i>m</i> -methoxy	6–6′	1.1 ± 0.1	1.0	0.9	0.9	71	37
6c	CH/N	CH/N	3,5-dimethoxy	6–6′	0.9 ± 0.2	2.3	1.5	1.5	93	49
6d	CH/N	CH/N	<i>p</i> -CF ₃	6–6′	1.0 ± 0.6	2	0.9	1.0	>50	52
6e	CH/N	CH/N	<i>p</i> -phenyl	6–6′	2.0 ± 0.6	13	2.1	2.0	>50	55
6f	CH/N	CH/N	<i>p</i> -CH ₂ -O-phenyl	6–6′	6.2 ± 0.8	17	27	32	>100	>100
6g	CH/N	CH/N	<i>p</i> -O-(2-F-phenyl)	6–6′	9.5 ± 1.4	8.2	5.3	5.5	>100	>100
6h	CH/N	CH/N	3,4-triazole ring ^d	6–6′	1.5 ± 0.3	2.5	6.6	9.4	>100	52
Benzimidazole Substitution										
10a	N/N	CH/N	<i>m</i> -methoxy	6–6′	6.0 ± 1.4	34	54	57	>100	>100
10b	CH/N	N/N	<i>m</i> -methoxy	6–6′	4.7 ± 1.0	45	56	63	>100	>100
10c	N/N	CH/N	<i>m</i> -methoxy	5–6′	3.8 ± 0.8	6	48	>100	>100	>100
10d	CH/N	N/N	<i>m</i> -methoxy	6–5′	5.3 ± 1.0	56	28	49	>100	>100
Alternative Benzyl Linkage										
14a	CH/N	NH/C	<i>m</i> -methoxy	6–6′	0.9 ± 0.2	6	5.6	5.8	33	24
14b	NH/C	CH/N	<i>m</i> -methoxy	6–6′	1.6 ± 0.4	7	18	18	57	34
14c	NH/C	NH/C	<i>m</i> -methoxy	6–6′	0.9 ± 0.2	4	5.9	6.2	500	12
16	NH/C	NH/C	<i>m</i> -COOMe	5–5′	1.2 ± 0.2	2	5.0	4.8	99	31

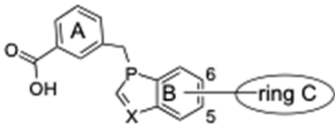
^a K_i : inhibition constant for hydrophobic pocket binding, in μM . ^bCCF: cell–cell fusion, Env subtype HXB2, performed in OptiMEM (0% serum), in μM . ^cVCF: virus–cell fusion (measured as viral replication), Env subtypes Ba-L and IIIB, 2% serum; in μM . ^dRing D is



(14b, 14c, 16, 18a, 18b); indole C was replaced with benzimidazole (10b, 10d), benzene (21a, 21b), or quinoline (22a, 22b); ring D was moved to the 3-position (14a); ring D was replaced with a proton (18a, 18b) or methyl group (19) or substituted with a variety of polar and nonpolar groups (6a–m). The connectivity between B and C was also varied (6o–q). These substitutions allowed us to explore variation of shape, charge, hydrophobic contact surface area, and polar interactions. These studies were intended to verify that the hydrophobic and electrostatic interactions of the inhibitors are specific, rather than being due to amorphous long-range electrostatic or nonspecific hydrophobic effects,²⁷ and to test the potential of the compounds to form additional hydrogen bonds. Many of the isomers were also expected to have improved druglike properties including a lower lipophilicity. The results are shown in Table 1 and detailed below.

Molecular Shape. The linkage between indoles B and C was examined as a means of changing the overall shape of the molecule. Rings B and C in 1a are linked through the 6–6'

carbons. Compounds with 5–6' (6o), 6–5' (6p), and 5–5' (6q) linkages were synthesized and evaluated. The activity data indicated that all three compounds had reduced activity compared to 1a, not only in hydrophobic pocket binding affinity (3–4 times less active) but also in cell–cell fusion and viral replication assays (4–20 times less active) (Table 1). Conformational space sampled by the isomeric forms 1a, 6o–q was examined by generating 20 low energy conformers of each compound using OMEGA2, version 2.5.1.4 (OpenEye, Inc.).^{28,29} A sample of three conformers of each compound is shown in Figure S2 (Supporting Information) to illustrate accessible shapes of the molecules. The 6–6' linked bisindole scaffold was able to adopt the most compact shape overall. The 5–5' isomer adopted the most extended solution conformations and was also the worst performing of the four isomers. Continued synthetic exploration was restricted to 6–6' linked indoles, which apparently better conform to the shape of the hydrophobic pocket.

Table 2. Biochemical and Cell-Based Assay Data in μM for Compounds with Three Aromatic Ring Systems


compd	X	P	link	ring C structure	K_i^a	EC ₅₀ fusion inhibition			TC ₅₀ toxicity	
						CCF HXB2 ^b	VCF Ba-L ^c	VCF IIIb ^b	resazurin ^b	MTS ^c
21a	CH	N	6	3-methoxyphenyl	4.9 ± 0.6	14	28	nd	>100	>100
21b	CH	N	6	3-hydroxyphenyl	2.6 ± 0.3	8	23	nd	~100	94
23	CH	N	6	6-indole	2.7 ± 0.2	15	60	47	>100	>50
18a	NH	C	5	6-indole	1.7 ± 0.3	5	13	13	194	80
18b	NH	C	6	6-indole	0.6 ± 0.1	6	13	14	290	23
22a	CH	N	6	2-(6-Cl-quinoline)	3.9 ± 0.6	13	48	nd	50	>100
22b	CH	N	5	2-(6-Cl-quinoline)	1.7 ± 0.3	8	6	nd	100	50
20a	N	N	6	6-indole	11 ± 2	14	41	36	>100	>100
20b	N	N	5	6-indole	16 ± 4	124	>100	>100	>100	>100
19	CH	N	6	6-(1-methylindole)	0.3 ± 0.1	1.3	4.5	4.3	>>50	>50

^a K_i : inhibition constant for hydrophobic pocket binding, in μM . ^bCCF: cell–cell fusion, Env subtype HXB2, performed in OptiMEM (0% serum), in μM . ^cVCF: viral replication, Env subtypes Ba-L and IIIb, 2% serum, in μM .

Hydrophobic Surface Area. Since the hydrophobic pocket is located on the long groove formed along the NHR, we next tested the effect of increasing van der Waals contacts by introducing additional hydrophobic substituents to ring D. Compounds **6e**, **6f**, and **6g** all contain an additional phenyl group attached to ring D, and compound **6h** has ring D replaced with a benzotriazole (Table 1). Activity did not improve, leading us to believe that optimization should focus on specific interactions in the hydrophobic pocket rather than on extending the contact surface area. We also could not rule out whether the compounds might exhibit lower potency due to lower solubility under the conditions of in vitro assays.

We then tested the effect of reduced compound size by eliminating ring D, which automatically reduces total surface area. Compounds **18a,b**, **19**, **20a,b**, **23** (Scheme 4) and four previously studied compounds **21a**, **21b**, **22a**, **22b**²² all contain three aromatic ring systems (Table 2). Compound **23**, the precursor of **6a–m**, demonstrated that ring D is essential for antiviral potency; it had an EC₅₀ of 60 μM against HIV-1 Ba-L, while our best four-aromatic system compound **6j** had 0.2 μM potency. Two of the compounds had submicromolar binding affinity: **18b** with a 3-substituted indole B and two free indole NH protons as well as **19** containing N-Me (Scheme 4), but this did not translate into submicromolar antiviral activity. The discrepancy between binding and fusion of compounds **18b** and **19** suggests that factors other than HP binding may play a role in inhibition in the biological milieu, either by a change in pocket shape or accessibility or by contribution of a secondary interaction.

In the context of three aromatic system compounds, the character of rings B and C were important, and binding affinity decreased in the order indole ≥ quinoline > phenyl > benzimidazole. Further examination was confined to compounds with four aromatic systems, given the inability of smaller compounds to yield submicromolar inhibition against viral fusion.

Polarity of the Indole Core. Benzimidazole replacement of either indole B or C was introduced (Scheme 2) as a way to increase polarity in the core of the scaffold without altering the shape of compounds with four aromatic systems. In addition, coupling of ring A and/or ring D to the 3' position of the indoles

was tested (Scheme 3), which leaves a free indole NH proton that could potentially make hydrogen bonds to residues of the protein.

Compounds **14a–c** and **16** with at least one free indole NH proton had low micromolar to submicromolar K_i values and moderate in vitro EC₅₀ values. Compound **16**, having shape equivalent to **6j** but with two free indole NH protons, forms a compact structure and is the most active of these variants. While binding affinity is similar, bioactivity is lower than for **6j**, and while it appears that 3-substitution does not significantly affect K_i , it is detrimental in the local environment of in situ gp41. By virtue of the 3-substituted indoles, compounds **14a**, **14b**, and **14c** have extended shapes similar to **6p**, **6o**, and **6q**, respectively, and have similar activity. Replacement of indole groups with benzimidazole increased K_i and practically abrogated antifusion activity entirely.

Substitution at Ring D. It is clear from Table 1 that addition of ring D to compound **23** ($K_i = 3 \mu\text{M}$) had a significant effect on compound potency, leading to K_i values as low as 0.6 μM or as high as 12 μM and over 2 orders of magnitude variation in fusion inhibitory activity.

Varying Small Nonpolar Substituents on Ring D Had a Small Effect on Compound Activity. We observed that *m*-methoxy (**6b**) or *p*-CF₃ (**6d**) substitution had no effect on binding affinity or potency, while a 3,5-dimethoxy substitution on ring D (**6c**) caused a barely perceptible decrease in biological activity but no change in binding affinity. Compound **6a** with unsubstituted ring D showed a 5-fold decrease in activity. Bulky additions to ring D, discussed earlier, compromised binding and antiviral potency compared to **1** (**6e–h**). We observed an overall agreement between cell–cell fusion and viral infectivity EC₅₀ values and, with the exception of compound **6e**, between K_i and EC₅₀^{CCF}. This suggests that a hydrophobic pocket binding mechanism is central to the potency of the compounds.

Polar Substituents on Ring D Had a Marked Effect in Decoupling K_i from EC₅₀^{CCF} and EC₅₀^{VCF}. In all cases, a carboxylate, an amide, or an ester as a meta substituent on ring D improved binding affinity to mostly submicromolar levels. However, carboxylic acid and amide groups in **6i** and **6m**³⁰ invariably resulted in significantly reduced activity against fusion. Conversely, retaining the methyl or ethyl ester resulted in

Table 3. Activity in nM of Leading Compounds in PBMC Assays^a

HIV-1 isolate	6j				6k				T20			
	EC ₉₀	EC ₅₀	TC ₅₀	TI	EC ₉₀	EC ₅₀	TC ₅₀	TI	EC ₉₀	EC ₅₀	TC ₅₀	TI
Ba-L (subtype B)	630	360	11 600	32.2	590	410	>50 000	>121	23.6	7.55	>2000	>265
92BR014 (subtype B)	1430	460	11 600	25.3	1230	430	>50 000	>116	>2000	>2000	>2000	N/A
01CM0005BBY (subtype CRF02_AG)	540	290	11 600	39.3	550	340	>50 000	>147	55.8	18.1	>2000	>110
02CM0015BBY (subtype CRF02_AG)	520	240	11 600	47.8	560	370	>50 000	>137	43.4	16.9	>2000	>118
91DJ263 (subtype CRF02_AG)	920	390	11 600	29.7	580	350	>50 000	>141	206	120	>2000	>16.6
00UG_D26830M4 (subtype D)	580	350	11 600	33.3	570	390	>50 000	>128	195	108	>2000	>18.6
92UG001 (subtype D)	990	400	11 600	29.1	1000	350	>50 000	>141	71.3	55.6	>2000	>36.0

^aTC₅₀: toxic concentration for 50% of the cells. TI (therapeutic index) = TC₅₀/EC₅₀; all values in nM.

enhanced fusion inhibitory activity that exceeded the K_i in potency by a factor of 2–3. This result suggests that the characteristics required for hydrophobic pocket binding in solution begin to deviate from those required for fusion inhibition below a 1 μ M threshold of potency. It is possible that the proximity of the membrane to the hydrophobic pocket of gp41 in situ modifies the requirements for a compound to bind effectively and inhibit fusion. In this scenario, a charge on ring D would have a deleterious effect on the ability of the compound to reach the site of action, while uncharged groups such as esters can still approach and bind tightly. We have observed that the indole inhibitors can partition into POPC/cholesterol liposomes, cells, and virus particles, with a reduced interaction for **6i** compared to **6b** (unpublished). Furthermore, the relationship between membrane partitioning and efficacy has been established for gp41 C-peptide inhibitors.³¹

Acid Esters on Ring D Yielded 200 nM Inhibition of Viral Replication and Also Inhibited T20-Resistant Virus. The best performing compounds **6j** and **6k** inhibited cell–cell fusion with EC₅₀^{CCF} = 200–700 nM and inhibited viral replication with EC₅₀^{VCF} = 200–300 nM. We measured the antiviral activity of the compounds against various primary strains of HIV-1 in PBMCs, finding that they retained high potency even against a T20 resistant strain (Table 3). The methyl ester containing compound **6j** gave EC₅₀ values in the range 250–460 nM, tested against six different strains of HIV-1, including a strain with T20 EC₅₀ > 2000 nM. For the ethyl ester **6k**, EC₅₀ values varied from 350 to 420 nM. Submicromolar EC₉₀ values were typically obtained. For two viral strains with partial insensitivity to T20, EC₅₀ values for **6j** and **6k** were only 3 times higher than for T20. Retention of activity against T20 resistant strains is an expected property of compounds targeting the hydrophobic pocket, since they do not overlap the binding surface of T20. It suggests that the hydrophobic pocket binders could be useful in combination therapy with T20. The mechanism of inhibition of HIV entry was further confirmed by studies showing that **6j** and **6k** had minimal effect in a MAGI attachment assay (Supporting Information Table S1 and Figure S3), which is performed with a washout of compound and unbound virus following a short-term incubation that coincides with the virus attachment and fusion steps of virus infection. Coupled with the results observed in the other assays, loss of compound activity in this assay indicates the virus is able to attach to cells in the presence of the compounds and continue with fusion and subsequent steps of virus infection and replication after the compounds are washed out of the assay.

Interpretation of SAR on the Ring Systems. The diversity of the compound set has allowed us to obtain an informative SAR data set and to evaluate potential binding modes of the compounds in the pocket. The low binding and fusion inhibitory properties of **20a** and **20b**, mirrored also in **10a** and **10c**, in which

ring B is benzimidazole, suggests that an indole group is desirable for ring B, which is likely to be buried in a hydrophobic part of the pocket. A lone-pair-containing nitrogen atom at the 3 position cannot be accommodated, in contrast to an indole NH that was tolerated (**14b**, **14c**, **16**). Similar functionality was required for ring C, suggesting that the bisindole core might anchor the compounds in the pocket. Variation of a factor of 20 in K_i and a factor of 250 in EC₅₀^{VCF} was observed for different ring D substituents, and methyl and ethyl esters were clearly favored. This fact points to an important role of ring D in conferring activity. Ring D was required for submicromolar in vitro potency against fusion, although it was not essential for submicromolar hydrophobic pocket binding.

On the basis of previous reports of the importance of salt-bridge interactions between peptide and small molecule inhibitors and pocket Lys574,^{32,33} we evaluated the binding affinity of select compounds to a mutant receptor in which Lys574 was replaced with norleucine (Nle). Nle contains the hydrophobic side chain of a Lys but is missing the ϵ -amino group. Binding affinity was slightly impaired by a factor of 2–3 (Supporting Information Table S2), which is within the range of experimental error of measurement of K_i , but was consistently observed for almost all the compounds measured. It appears likely that a specific salt bridge between Lys574 and the ligand carboxylate, if it exists, does not contribute substantially to potency. We have seen this previously with peptides and other small molecules.^{27,34}

Prediction of Bound Conformation. Evaluation of binding modes is complicated by the variability of the gp41 hydrophobic pocket in the available Protein Data Bank (PDB) structures. Pockets containing small molecules, peptides or antibodies show significant side chain variations,³⁵ and it is likely that binding of the indole compounds would result in induced fits that are difficult to predict a priori. Interestingly, most gp41 structures in the PDB have a pocket structure that is not large enough to accommodate compounds with four aromatic systems fully within the groove. The exception to this is the structure 2XRA, which has an antibody HK20 bound to it.³⁶ We investigated the poses and calculated affinities of the compounds listed in Tables 1 and 2 using FRED 2.2.5 OEDocking software (OpenEye, Inc.), which includes options to analyze poses using a variety of scoring functions. We used scoring functions OECheScore, ShapeGauss, Piecewise Linear Potential, Zapbind, Screenscore, and ChemGauss3 to evaluate the lowest energy pose and 20 alternative conformations of each ligand. These energy functions are described in detail in FRED documentation and are briefly explained in the Supporting Information. Because of the much lower dynamic range of K_i and EC₅₀^{CCF} data compared to EC₅₀^{VCF}, we used the latter as a more discriminating data set to distinguish between different poses and structures.

The Lowest Energy Consensus Pose of 6–6' Linked Bisindoles in 2XRA Showed Excellent Correlation to Experimental Data. Extensive HK20 side chain interactions in and surrounding the hydrophobic pocket create a large core cavity for accommodating a ligand in 2XRA. In this structure we obtained a highly consistent lowest energy consensus pose for almost all 6–6' four-ring compounds, shown in Figure 2A. We consistently

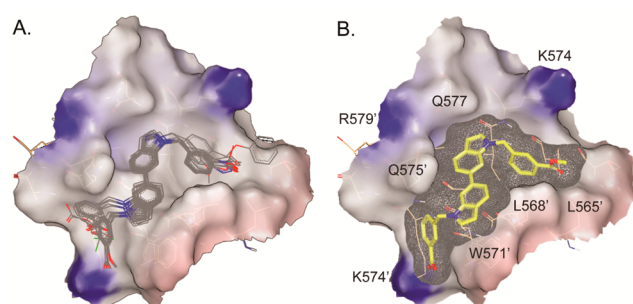


Figure 2. Four-ring system compounds with 6–6' bisindole and 1,1'-benzyl linkages, docked using FRED 2.2.5 into PDB structure 2XRA (five-helix, antibody HK20 binding site). (A) Shown overlaid are 1a, 6a–d, 6f, 6h–k, 10a–b. (B) 6j docked in the binding site.

found the best correlation to experimental data using OEChemScore. OEChemScore is a modification of Chemscore,³⁷ using simple contact terms to define lipophilic interactions, an explicit term for hydrogen bonds, and a penalty for clashes between protein and ligand. This scoring function sums over the pairwise interactions between ligand and protein and is likely to reflect the total contact area between them. Figure 3 shows the calculated

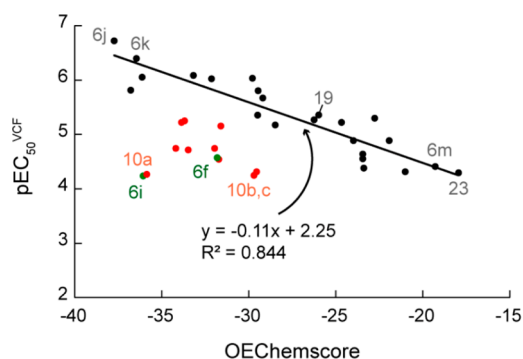


Figure 3. OEChemScore plotted against observed EC_{50}^{VCF} for molecules in Tables 1 and 2. Scores of the lowest energy conformer selected by FRED docking are included for three categories described in the text: (1) 6–6' linked bisindole compounds, 3-substituted bisindoles with complementary shape, and all three-ring systems (black); (2) benzimidazole containing compounds and alternatively linked bisindole compounds (red); (3) outliers not included in the calculation of correlation coefficient (green). The data for this graph are provided in the Supporting Information.

OEChemScore values for the lowest energy conformer, plotted against pEC_{50}^{VCF} . Compounds were separated into three categories based on the observed results: (1) 6–6' four-ring systems not containing benzimidazole, and all three-ring systems; (2) benzimidazole-containing compounds and alternatively linked four-ring compounds; and (3) two outliers 6f and 6i not included in the previous two categories. A remarkable correlation coefficient $R^2 = 0.844$ was obtained for category 1, which included most of the compounds in our data set (23

compounds). Category 2 is a miscellaneous combination of 11 compounds with different shapes and charge distribution, as a result of which they gave a variety of different bound poses and there was insufficient sampling within each subgroup to reach detailed conclusions. It is clear, however, that these compounds are predicted to be more active than what was found experimentally, which could be a result of bioavailability considerations or a flexible receptor structure. In this context, the poor activity of benzimidazole derivatives is not understood.

Observed K_i and antiviral activity of 6i and 6m showed the greatest discrepancy of all compounds, and this was mirrored in the calculation for 6i, which adopts the same pose as 6j (Figures 2 and 3). Interestingly, a similar observation of low antiviral activity for compounds containing two carboxylates, and much improved activity for the methyl ester, was obtained in a recent study of elongated pyrrole-thiazolidinyl containing compounds.¹⁹ Carbo-methoxy substituents on a terminal benzyl ring were at least 10 times more active ($EC_{50}^{CCF} = 1.8 \mu M$) than the corresponding free carboxylic acid ($EC_{50}^{CCF} = 21–68 \mu M$). It is possible that the loss of potency is due to the local lipophilic environment of in situ gp41, since 6i binds strongly to gp41 in solution and is not an outlier in correlations with pK_i . Compound 6m formed an internal H-bond in the calculations and could not assume the extended pose shown in Figure 2A. The compact pose made far fewer contacts with the protein surface, consequently resulting in poor calculated activity, which correlated with its poor VCF activity. The remaining outlier is 6f, a five-ring compound in which the extensive contact area with the protein is not matched by experimental efficacy. With such compounds, solubility could play a role in the diminished potency. A few additional outliers were found in the pK_i correlation (Supporting Information Table S3 and Figure S4), but this is not considered as reliable because of the available low dynamic range.

In the bound pose in 2XRA in Figure 2B, compounds 6j and 6k, were the top ranked compounds and they are clearly also the most potent compounds experimentally. They ranked at positions 1 and 3 in the data set of 36 compounds. In fact, several scoring functions ranked these compounds at or near to top of the list. Table S3 shows the calculated correlation coefficients for all scoring functions and the rank of the top compounds. Five of the six scoring functions yielded correlation coefficients $R^2 > 0.53$ with VCF data, and 6j was ranked as the top scoring compound using OEChemScore, Shapegauss, Piecewise Linear Potential, and Chemgauss3; 6k ranked third, second, ninth, and sixth, respectively, out of 36 compounds. This encourages us to believe that the pose found in 2XRA (Figure 2B) is independent of scoring function and may well represent an accurate pose.

CONCLUSIONS

In this study, we designed, synthesized, and tested a series of indole derivatives as entry inhibitors against gp41-mediated HIV-1 fusion. SAR studies revealed a defined shape, charge, and hydrophobic contact surface required to fit into the hydrophobic pocket. Optimization resulted in improved binding affinity, viral replication, and cell–cell fusion inhibition, with several compounds having submicromolar activity and the most active compound 6j exhibiting binding affinity with K_i of $0.6 \mu M$ and EC_{50} of $0.2 \mu M$ in cell–cell fusion inhibition and viral replication inhibition. A computational pose was obtained that explained the observed SAR.

We found that submicromolar inhibition constants for binding to the hydrophobic pocket on the gp41 coiled coil were a

necessary but not sufficient condition for observing submicromolar inhibition of cell–cell and virus–cell fusion. Below $K_i = 1 \mu\text{M}$, the correlation between K_i and EC_{50} was diminished, indicating a factor other than hydrophobic pocket binding required for fusion inhibition. Polar and nonpolar groups at opposite ends of the elongated molecules were a dominant feature of submicromolar fusion inhibitors, but compounds containing polar groups at both ends were poor fusion inhibitors while equally potent HP binders. We surmise that proximity of the target to lipid membranes may influence accessibility of the pocket and bioavailability of the inhibitors, given the lipophilic character of the best inhibitors. Future work will focus on improving the therapeutic index and understanding the mechanism that yields submicromolar activity in cell culture.

■ EXPERIMENTAL SECTION

Chemistry. Starting materials and solvents were purchased from commercial sources and used as is. HPLC was performed on a Waters Breeze HPLC with multiwavelength fluorescence detector and dual wavelength UV detector, using a water/acetonitrile or water/methanol gradient with 0.05% TFA. Mass spectra were obtained on LCMS instrument (Finnigan LCQ Duo, H_2O /methanol gradient with 0.1% formic acid) by ESI or by high-resolution mass spectrometry (HRMS) on a ThermoFisher Orbitrap XL (UC Davis). ^1H NMR and ^{13}C NMR spectra were collected on a Bruker spectrometer at 400 and 100 MHz, respectively, in $\text{DMSO}-d_6$ unless otherwise stated and calibrated using the residual solvent signal. Multiplicities are abbreviated as follows: s = singlet, d = doublet, t = triplet, q = quartet, m = multiplet, and br = broad. Where consistent coupling constants have been observed in the NMR spectrum, the apparent multiplicity of the proton signal concerned is reported.

Flash column chromatography was carried out with Silicycle SiliaFlash P60 40–63 μm silica gel. Reactions and chromatography fractions were monitored with Sorbent Technologies silica gel 60 F_{254} TLC plates and visualized using UV light. Reactions were carried out under inert gas atmosphere in oven-dried glassware, and reaction solutions were magnetically stirred. All other reagents and solvents were used without further purification from commercial sources unless otherwise noted. All target compounds were purified by preparative HPLC or analyzed by HPLC to ensure $\geq 95\%$ purity.

The organic synthesis was carried out according to Schemes 1–4 and Scheme S1 in the Supporting Information. Representative synthetic procedures for the preparation of compounds **4**, **5**, **6b**, **6i**, **6j**, **6k**, **6m**, **11a**, **12a**, **19**, and **23** are described below. Characterization data for other target compounds and synthetic intermediates are provided in the Supporting Information.

Synthesis of Methyl 3-[(6-Bromoindol-1-yl)methyl]benzoate (4). To a solution of methyl 3-(bromomethyl)benzoate **3a** (458 mg, 2.00 mmol) and 6-bromoindole **2a** (382 mg, 1.95 mmol) in dry DMF (5.0 mL) was added K_2CO_3 (1.38 g, 10.0 mmol). The mixture was stirred at room temperature overnight. TLC indicated no starting material remained; the reaction was quenched by adding 25 mL of water. The solution was extracted with ethyl acetate (30 mL \times 3). The organic solvent was combined and evaporated, and the product was purified by silica gel chromatography using EtOAc/hexane (15:85) as eluent. 655.2 mg of target compound was achieved as a pale yellow oil, 95%. ^1H NMR δ 7.86 (d, $J = 7.6$ Hz, 1H), 7.79 (s, 1H), 7.41 (d, $J = 8.4$ Hz, 1H), 7.31 (s, 1H), 7.27 (t, $J = 8.0$ Hz, 1H), 7.14–7.06 (m, 2H), 7.00 (d, $J = 3.2$ Hz, 1H), 6.45 (d, $J = 3.2$ Hz, 1H), 5.20 (s, 2H), 3.81 (s, 3H); ^{13}C NMR δ 166.99, 137.74, 137.32, 131.41, 131.08, 129.40, 129.11, 128.20, 127.91, 123.32, 122.61, 115.81, 114.25, 112.81, 102.66, 52.58, 50.09.

Synthesis of Methyl 3-[(6-(1H-Indol-6-yl)indol-1-yl)methyl]benzoate (5). To a solution of indole-6-boronic acid (274 mg, 1.7 mmol) and compound **4** (516 mg, 1.5 mmol) in THF (15 mL) was added $\text{Pd}(\text{PPh}_3)_4$ (87.2 mg, 0.075 mmol), followed by K_2CO_3 (2.0 M, 3.0 mL). The mixture was stirred and heated to reflux under argon for about 4 h. After the reaction was completed, the mixture was cooled to room temperature, water (20.0 mL) was added, and the product was

extracted with ethyl acetate (20 mL \times 3). The organic solvent was combined, dried over anhydrous Na_2SO_4 , filtered, and evaporated. The crude product was purified by silica gel chromatography (20% EtOAc/hexanes). 380.1 mg target compound was obtained as a pale yellow oil, 67%. MS calculated for $\text{C}_{25}\text{H}_{20}\text{N}_2\text{O}_2$, 380.2; found, 381.1 ($\text{M} + \text{H}^+$); ^1H NMR δ 8.19 (br, 1H), 7.97 (s, 1H), 7.93 (d, $J = 7.8$ Hz, 1H), 7.68 (dd, $J = 12.8$ Hz, $J = 8.2$ Hz, 2H), 7.58 (s, 1H), 7.49 (s, 1H), 7.44 (d, $J = 8.2$ Hz, 1H), 7.39 (d, $J = 8.0$ Hz, 1H), 7.34 (t, $J = 7.6$ Hz, 1H), 7.25 (br, 1H), 7.20 (t, $J = 2.4$ Hz, 1H), 7.14 (d, $J = 3.0$ Hz, 1H), 6.59 (d, $J = 3.0$ Hz, 1H), 6.56 (br, 1H), 5.40 (s, 2H), 3.89 (s, 3H); ^{13}C NMR δ 167.14, 138.32, 137.16, 137.01, 136.94, 136.79, 131.64, 130.97, 129.36, 129.22, 128.82, 128.39, 127.98, 127.69, 127.12, 123.32, 122.61, 115.81, 114.25, 110.16, 108.56, 102.68, 102.27, 52.56, 50.07.

Synthesis of 3-[[6-[1-[(3-Methoxyphenyl)methyl]indol-6-yl]indol-1-yl]methyl]benzoic Acid (6b). To a stirred solution of compound **5** (19 mg, 0.05 mmol) in anhydrous DMF (3.0 mL) at 0°C was added sodium hydride in oil (60%, 15 mg), and the reaction mixture was allowed to warm to rt over 60 min. 3-Methoxybenzyl bromide (10.5 mg, 0.052 mmol) was added, and the mixture was stirred at room temperature overnight. The reaction was quenched by adding 10 mL of water. The solution was extracted with ethyl acetate (15 mL \times 3). The organic solvent was combined and evaporated; the crude product (22.5 mg, 90%) was directly used for saponification by adding 5.0 mL of 4.0 M NaOH and stirring for 1 h, and neutralized by adding 2.0 M HCl to pH 3.0. The solution was extracted with ethyl acetate (15 mL \times 3), and the organic solvent was combined and concentrated. 8.5 mg purified target compound was obtained by HPLC as a gray powder. Data for **6b**: MS calculated for $\text{C}_{32}\text{H}_{26}\text{N}_2\text{O}_3$, 486.2; found, 485.1 ($\text{M} - \text{H}^-$); ^1H NMR δ 7.82 (d, $J = 8.5$ Hz, 2H), 7.68 (d, $J = 7.8$ Hz, 2H), 7.60 (t, $J = 7.8$ Hz, 2H), 7.52 (d, $J = 2.9$ Hz, 2H), 7.46 (m, 2H), 7.35 (m, 2H), 7.20 (t, $J = 7.3$ Hz, 1H), 6.78 (m, 3H), 6.51 (d, $J = 2.8$ Hz, 1H), 6.48 (d, $J = 2.8$ Hz, 1H), 5.58 (s, 2H), 5.45 (s, 2H), 3.67 (s, 3H).

3-[[6-[1-[(3-Carboxyphenyl)methyl]indol-6-yl]indol-1-yl]methyl]benzoic Acid (6i). To a solution of compound **23** (19 mg, 0.05 mmol) in anhydrous DMF (3.0 mL) at 0°C was added sodium hydride in oil (60%, 15 mg), and the reaction mixture was allowed to warm to rt over 60 min. Methyl 3-(bromomethyl)benzoate (11.9 mg, 0.052 mmol) was added, then the mixture was stirred at room temperature overnight. Saponification was achieved by adding 5.0 mL of 4.0 M NaOH and stirring for 1 h. The reaction was neutralized by adding 2.0 M HCl to pH 3.0 and then extracted with ethyl acetate (15 mL \times 3). The organic solvent was combined and evaporated; the crude product (23.0 mg, 92%) was purified by HPLC. 15.5 mg of target compound was obtained as a yellow powder. Data for **6i**: MS (HRMS) calculated for $\text{C}_{32}\text{H}_{24}\text{N}_2\text{O}_4$ ($\text{M} - \text{H}$), 499.1652; found, 499.1648 ($\text{M} - \text{H}^-$); ^1H NMR δ 12.85 (s, 2H), 7.82 (br, 4H), 7.68 (s, 2H), 7.60 (d, $J = 8.5$ Hz, 2H), 7.52 (s, 2H), 7.45 (m, 4H), 7.36 (d, $J = 8.0$ Hz, 2H), 6.51 (s, 2H), 5.57 (s, 4H); ^{13}C NMR δ 167.0, 138.8, 136.4, 135.0, 131.3, 131.2, 129.5, 128.8, 128.2, 127.8, 127.2, 120.7, 119.0, 108.0, 101.0, 48.6.

3-[[6-[1-[(3-Methoxycarbonylphenyl)methyl]indol-6-yl]indol-1-yl]methyl]benzoic Acid (6j). To a stirred solution of **23** (232 mg, 0.632 mmol) in DMF (7.0 mL) at 0°C was added NaH (60% in mineral oil, 61.5 mg, 1.54 mmol), and the reaction mixture was allowed to warm to rt over 30 min. Methyl 3-(bromomethyl)benzoate (145 mg, 0.633 mmol) was added, and the mixture was stirred at room temperature overnight. The reaction mixture was quenched by adding 2.0 M HCl (20 mL), extracted with DCM (30 mL \times 3), and the combined organic fractions were concentrated. Purification by silica gel chromatography (40% \rightarrow 50% \rightarrow 60% EtOAc/hexanes) afforded **6j** (249 mg, 76%) as a light-brown oil. Data for **6j**: $R_f = 0.13$ (40% EtOAc/hexanes); MS (HRMS) calculated for $\text{C}_{33}\text{H}_{25}\text{N}_2\text{O}_4$ ($\text{M} - \text{H}^-$), 513.1809; found, 513.1803; ^1H NMR (CDCl_3) δ 10.68 (br, 1H), 7.99 (m, 3H), 7.91 (d, 1H, $J = 7.7$ Hz), 7.69 (d, 2H, $J = 8.3$ Hz), 7.46 (s, 2H), 7.41 (d, 2H, $J = 8.3$ Hz), 7.34–7.18 (m, 4H), 7.11 (d, 1H, $J = 3.0$ Hz), 7.09 (d, 1H, $J = 3.0$ Hz), 6.57 (m, 2H), 5.35 (s, 2H), 5.33 (s, 2H), 3.86 (s, 3H); ^{13}C NMR (CDCl_3) δ (5 pairs of signals are overlapping) 171.7, 167.0, 138.4, 138.2, 137.0, 136.9, 136.8, 132.3, 131.5, 130.7, 130.0, 129.6, 129.3, 129.1, 129.0, 128.8, 128.7, 128.3, 127.9, 121.3, 120.31, 120.29, 108.4, 102.2, 102.1, 52.4, 49.8, 49.7.

3-[[6-[1-[(3-Ethoxycarbonylphenyl)methyl]indol-6-yl]indol-1-yl]methyl]benzoic Acid (6k). To a stirred solution of **23** (107 mg, 0.292 mmol) in DMF (3.0 mL) at 0 °C was added NaH (60% in mineral oil, 30.2 mg, 0.755 mmol), and the reaction mixture was allowed to warm to rt over 30 min. Ethyl 3-(bromomethyl)benzoate (73 mg, 0.30 mmol) was added, and the mixture was stirred at room temperature overnight. The reaction mixture was quenched by adding 2.0 M HCl (10 mL), extracted with DCM (30 mL \times 3), and the combined organic fractions were concentrated. Purification by silica gel chromatography (40% \rightarrow 50% EtOAc/hexanes) afforded **6k** (128 mg, 83%) as a light-brown oil. Data for **6k**: R_f = 0.48 (50% EtOAc/hexanes); MS (ESI) calculated for $C_{34}H_{26}N_2O_4$ ($M - H$)⁻, 527.1965; found, 527.1963; ¹H NMR (CDCl₃) δ 8.04 (m, 3H), 7.97 (d, 1H, J = 7.8 Hz), 7.73 (m, 2H), 7.50 (s, 2H), 7.44 (d, 2H, J = 8.0 Hz), 7.41–7.30 (m, 3H), 7.23 (d, 1H, J = 7.9 Hz), 7.17 (d, 1H, J = 3.1 Hz), 7.15 (d, 1H, J = 3.1 Hz), 6.61 (m, 2H), 5.43 (s, 2H), 5.41 (s, 2H), 4.38 (q, 2H, J = 7.2 Hz), 1.39 (t, 3H, J = 7.2 Hz); ¹³C NMR (CDCl₃) δ (2 pairs of signals are overlapping) 171.6, 166.6, 138.4, 138.1, 137.01, 136.99, 136.93, 136.8, 132.3, 131.4, 131.1, 130.0, 129.7, 129.3, 129.1, 129.0, 128.8, 128.70, 128.67, 128.9, 127.9, 121.35, 121.33, 120.36, 120.31, 108.5, 102.2, 102.1, 61.4, 49.88, 49.85, 14.5.

Synthesis of 3-[[6-[1-[(3-Carbamoylphenyl)methyl]indol-6-yl]indol-1-yl]methyl]benzoic Acid (6m). To a stirred solution of compound **6l** (4.8 mg, 0.01 mmol) in DMSO (1.0 mL) cooled in an ice–water bath were added H₂O₂ (30%, 20.0 μ L) and K₂CO₃ (10.0 mg). The mixture was allowed to warm to room temperature. Then distilled water was added, extracted with DCM (10 mL \times 3). Purified by HPLC. After lyophilization, 2.4 mg of compound was achieved as an off-white powder. MS calculated for $C_{32}H_{25}N_3O_3$: 499.2. LCMS: 498.1 ($M - H$)⁻. ¹H NMR δ 7.81–7.78 (br, 3H), 7.67 (s, 2H), 7.56–7.51 (m, 3H), 7.41 (br, 3H), 7.33–7.26 (m, 5H), 6.49 (s, 1H), 6.45 (s, 1H), 5.55 (s, 2H), 5.51 (s, 2H).

Methyl *m*-[(6-Bromo-1*H*-indol-3-yl)methyl]benzoate (11a). To a vigorously stirred solution of 6-bromoindole (**2b**) (390 mg, 1.99 mmol) in toluene (8.0 mL) was added tetrabutylammonium iodide (367 mg, 0.994 mmol), Zn(OTf)₂ (450 mg, 1.24 mmol), followed by DIPEA (0.36 mL, 2.1 mmol). After the suspension was stirred for 20 min, methyl 3-bromomethylbenzoate (231 mg, 1.01 mmol) was added and the reaction mixture was stirred overnight. Reaction mixture was diluted with EtOAc (50 mL), water (10 mL), and saturated aqueous NH₄Cl (30 mL). The organic phase was separated and washed with water (30 mL) and brine (10 mL) and then concentrated. Purification by silica gel chromatography (15% \rightarrow 25% EtOAc/hexanes) afforded **11a** (338 mg, 97%) as a pink oil. Data for **11a**: R_f = 0.07 (15% EtOAc/hexanes); MS calculated for $C_{17}H_{13}^{79}BrNO_2$ ($M - H$)⁻, 342.01; found, 342.01; ¹H NMR (CDCl₃) δ 8.39 (br s, 1H), 8.04 (s, 1H), 7.95 (d, 1H, J = 7.6 Hz), 7.47 (m, 2H), 7.38 (d, 1H, J = 7.6 Hz), 7.35 (d, 1H, J = 8.1 Hz), 7.20 (dd, 1H, J_1 = 8.4 Hz, J_2 = 1.7 Hz), 6.86 (d, 1H, J = 2.2 Hz), 4.12 (s, 2H), 3.93 (s, 3H); ¹³C NMR (CDCl₃) δ 167.6, 141.5, 137.3, 133.4, 130.2, 129.8, 128.6, 127.4, 126.2, 123.4, 122.6, 120.2, 115.6, 115.0, 114.3, 52.2, 31.3.

***tert*-Butyl 6-Bromo-3-[(*m*-methoxycarbonylphenyl)methyl]-1*H*-indole-1-carboxylate (12a).** To a stirred solution of **11a** (338 mg, 0.982 mmol) in THF (9.0 mL) were added Boc₂O (0.24 mL, 1.04 mmol) and DMAP (10.0 mg), and the mixture was stirred overnight. Concentration and purification by silica gel chromatography (10% EtOAc/hexanes) afforded **12a** (429 mg, 98%) as a colorless oil. Data for **12a**: R_f = 0.32 (10% EtOAc/hexanes); MS (ESI) calculated for $C_{22}H_{23}^{79}BrNO_4$ ($M + H$)⁺, 444.08; found, 444.08; ¹H NMR (CDCl₃) δ 8.34 (br s, 1H), 7.96 (s, 1H), 7.89 (d, 1H, J = 7.8 Hz), 7.43 (d, 1H, J = 7.6 Hz), 7.34 (m, 2H), 7.26 (dd, 1H, J_1 = 8.4 Hz, J_2 = 1.9 Hz), 7.18 (d, 1H, J = 8.4 Hz), 4.03 (s, 2H), 3.89 (s, 3H), 1.67 (s, 9H); ¹³C NMR (CDCl₃) δ 167.1, 149.4, 139.9, 136.5, 133.2, 130.5, 129.8, 129.1, 128.7, 127.8, 125.8, 124.2, 120.5, 119.4, 118.6, 118.3, 84.2, 52.2, 31.2, 28.2.

3-[[6-(1-Methylindol-6-yl)indol-1-yl]methyl]benzoic Acid (19). To compound **5** (19 mg, 0.05 mmol) in anhydrous DMF (2.0 mL) were added iodomethane (35 mg, 0.25 mmol) and NaOH (20.0 mg). The mixture was stirred overnight, quenched by H₂O (10.0 mL), then adjusted to pH 3.0 using HCl (2.0 M). The solution was extracted with CH₂Cl₂ (10 mL \times 3). The organic solvent was combined and dried, then evaporated. Part of the crude product (16.2 mg, 84%) was purified

by HPLC; 2.4 mg of target compound was obtained as a yellow powder. MS calculated for $C_{23}H_{20}N_2O_2$: 380.2. LCMS: 379.2 ($M - H$)⁻. ¹H NMR δ 7.85 (s, 1H), 7.81 (d, J = 7.6 Hz, 1H), 7.77 (s, 1H), 7.64–7.61 (m, 2H), 7.57 (d, J = 8.0 Hz, 1H), 7.52 (d, J = 3.2 Hz, 1H), 7.46–7.41 (m, 3H), 7.35 (dd, J = 8.0 Hz, J = 1.6 Hz, 1H), 7.30 (d, J = 2.8 Hz, 1H), 6.52 (d, J = 2.8 Hz, 1H), 6.41 (d, J = 2.8 Hz, 1H), 5.59 (s, 2H), 3.84 (s, 3H).

3-[[6-(1*H*-Indol-6-yl)indol-1-yl]methyl]benzoic Acid (23). To a vigorously stirred solution of compound **5** (444 mg, 1.17 mmol) in THF/MeOH (4:1, 20.0 mL) was added aq NaOH (25%, 5.0 mL). The mixture was stirred at room temperature for 3 h, then quenched with 3.0 M HCl (24 mL), extracted with DCM (50 mL \times 3), dried, filtered, and concentrated. Purification by silica gel chromatography (10:1 DCM/MeOH) afforded **23** (400 mg, 93%) as an off-white solid. Data for **23**: R_f = 0.13 (40% EtOAc/hexanes); MS (ESI) calculated for $C_{24}H_{17}N_2O_2$ ($M - H$)⁻, 365.13; found, 365.13; ¹H NMR (DMSO-*d*₆) δ 12.87 (s, 1H), 11.02 (s, 1H), 7.75 (m, 2H), 7.66 (s, 1H), 7.55 (m, 3H), 7.47 (d, J = 4.0 Hz, 1H), 7.40 (m, 2H), 7.28 (m, 3H), 6.46 (d, J = 3.1 Hz, 1H), 6.36 (s, 1H), 5.54 (s, 2H); ¹³C NMR (DMSO-*d*₆) δ 167.1, 139.1, 136.6, 136.5, 135.5, 134.7, 131.4, 131.1, 129.5, 128.9, 128.2, 127.7, 127.2, 126.6, 125.8, 120.8, 120.2, 119.0, 118.8, 109.4, 108.1, 101.1, 100.9, 48.6.

Binding Affinity Assay. Inhibition constants K_i for binding in the hydrophobic pocket were determined using a fluorescence intensity assay as previously described.^{38,39} Briefly, Fe^{II}(env2.0)₃ was used to mimic the hydrophobic pocket in the gp41 NHR coiled coil. Env2.0 contains 20 hydrophobic pocket-associated residues (₅₆₅LLQLTVWG-₅₈₄IKQLQARILAVE₅₈₄). It is N-terminally capped by 2,2-bipyridine-5-carboxylate, a bidentate ferrous iron chelator that ensures the trimeric structure of the NHR upon metal binding. A fluorescein (FL) labeled pocket-binding C-peptide C18FL was used to probe inhibitor binding. Quenching of probe fluorescence occurred in the presence of Fe^{II}(env2.0)₃. K_i was determined by measuring the dose dependent fluorescence recovery in the presence of a competitive inhibitor. A modified metalloprotein construct with K₅₇₄ replaced with norleucine was employed to measure the effect of the lysine side chain amino group on inhibitor binding affinity.

Cell–Cell Fusion Assay. Cell–cell fusion was measured as previously published²² and using cell lines obtained through the NIH AIDS Research and Reference Reagent Program, Division of AIDS, NIAID, NIH. Target cells were TZM-bl cells (no. 8129, contributed by J.C. Kappes, X. Wu, and Tranzyme Inc.) expressing CD4, CCR5, and CXCR4,⁴⁰ and containing an integrated reporter gene for firefly luciferase under control of HIV-1 LTR.⁴¹ Effector cells were HL2/3 (no. 1294, contributed by B. K. Felber and G. N. Pavlakis) which produce HXB2 Env, Tat, and Rev.⁴² Serially diluted inhibitors were added to 96-well plates containing 25 000 TZM-bl cells per well cultured overnight. 50 000 HL2/3 cells were added per well, and fusion was allowed to proceed for 6 h in reduced serum medium (Gibco) with a final concentration of 1% DMSO. Luciferase expression was measured using luciferase assay reagent (Promega) according to the manufacturer's instructions. Controls containing 1 μ L of DMSO with and without HL2/3 cells were measured for each compound, and experiments were performed in triplicate.

Viral Replication and Attachment Assays. Inhibition of HIV-1 replication was determined in CCR5- and CXCR4-tropic MAGI antiviral assays, and inhibition of HIV-1 attachment/entry was determined in CCR5-tropic MAGI attachment assays as previously described.^{43,44} HIV-1 isolates and cells were obtained from the NIH AIDS Research and Reference Reagent Program, Division of AIDS, NIAID, NIH, as follows: HIV-1 Ba-L from Suzanne Gartner, Mikulas Popovic, and Robert Gallo.^{44,45} HIV-1 IIIB from Robert C. Gallo.^{44,46} MAGI-CCR5 cells from Dr. Julie Overbaugh.^{47,48} For MAGI antiviral assays, MAGI-CCR5 cells were grown overnight in 96-well plates in DMEM supplemented with 10% FBS, using 10 000 cells per well. The following day the medium was removed and compounds diluted in medium were added (six dilutions in triplicate at each dilution), followed by the addition of either HIV-1 Ba-L (CCR5-tropic assay) or HIV-1 IIIB (CXCR4-tropic assay) at approximately 10 50% tissue culture infective doses per well (\sim 10 TCID₅₀/well). Assay plates were incubated for 48 h, after which medium was removed and HIV-1 Tat-

induced β -Gal enzyme expression was determined by chemiluminescence using Tropic Gal-Screen (Applied Biosystems) according to the manufacturer's instructions. MAGI attachment assays were performed similarly but with a washout of unbound virus and compounds 3 h postinfection. Assays were conducted at a serum concentration of 2%.

HIV-1 PBMC Assay. Testing of compounds against HIV-1 in PBMCs was performed as previously described.⁴⁹ PBMCs were isolated from blood of screened donors (Biological Specialty Corp., Colmar, PA) by Ficoll gradient purification and stimulated using 4 μ g/mL phytohemagglutinin and subsequently maintained in media containing 20 U/mL of IL-2. Cells from two donors were mixed, adjusted to 1×10^6 cells/mL, and added to 96-well round-bottom plates at 50 μ L/well (5×10^4 cells/well). Test compound dilutions (nine total serial dilutions) were prepared in media at 2X concentrations and added to triplicate wells at 100 μ L/well followed by the addition of a predetermined dilution of virus stock at 50 μ L/well (final multiplicity of infection [MOI] of ~ 0.1). Antiviral efficacy was determined 6 days later based on supernatant reverse transcriptase (RT) activity using a microtiter plate-based RT reaction.⁵⁰ The following virus isolates were obtained from the NIH AIDS Research and Reference Reagent Program, Division of AIDS, NIAID, NIH: HIV-1 isolates 92BR014 (catalog no. 1753) and 92UG001 (catalog no. 1647) from The UNAIDS Network for HIV Isolation and Characterization;⁵¹ HIV-1 isolates CAM0005BBY (catalog no. 11278), CAM0015BBY (catalog no. 11282), and D26830M4 (catalog no. 11264) from Dr. Victoria Polonis;⁵² HIV-1 91DJ263 (catalog no. 7685) from Dr. Nelson Michael;⁵³ and HIV-1 Ba-L as noted above.

Cytotoxicity Assay. The cytotoxic effect of the compounds was determined using the cell culture procedure identical to that described above for viral replication or cell–cell fusion but measuring cell viability using 3-(4,5-dimethylthiazol-2-yl)-5-(3-carboxymethoxyphenyl)-2-(4-sulfophenyl)-2H-tetrazolium (MTS, CellTiter 96 reagent; Promega; used for MAGI and PBMC assays) or using a resazurin cell viability reagent (Alamar Blue or Presto Blue, Life Technologies; used for cell–cell fusion assays) following the manufacturers' protocols.

Cheminformatics and Computational Docking. The OpenEye software suite (OpenEye Scientific Software, Santa Fe, NM, <http://www.eyesopen.com>) was used for ligand analysis, conformer predictions, compound overlays, and computational docking. Charges and 3D coordinates of each ligand were generated from SMILES strings using OMEGA2, version 2.5.1.4.^{28,29} Compound overlays were created using ROCS, version 3.1.2.^{54,55} Multiconformer representations of each ligand were docked into the receptor 2XRA (Protein Data Bank) using the OEDocking utility and FRED, version 2.2.5.⁵⁶ Twenty alternative docked poses were retained for each ligand.

■ ASSOCIATED CONTENT

■ Supporting Information

(1) Synthetic procedures and compound characterization not described in Experimental Section; (2) sample solution conformations of bisindole compounds; (3) MAGI attachment assay results, binding affinities to mutant receptor L574Nle, data and correlation coefficients for calculated vs observed activity. This material is available free of charge via the Internet at <http://pubs.acs.org>.

■ AUTHOR INFORMATION

Corresponding Author

*Phone: 707-638-5463. Fax: 707-638-5255. E-mail: miriam.gochin@tu.edu.

Notes

The authors declare no competing financial interest.

■ ACKNOWLEDGMENTS

This work was supported by NIH Grants AI093243 and GM087998 to M.G. and internal funds from Southern Research Institute. We thank S. Chu for assistance with running ROESY

spectra of benzimidazole compounds. Molecular graphics images were produced using the UCSF Chimera package from the Resource for Biocomputing, Visualization, and Informatics at the University of California—San Francisco (supported by NIH Grant P41 RR-01081) or using Vida, version 4.2.1 (OpenEye Scientific Software, Inc.).

■ ABBREVIATIONS USED

HIV, human immunodeficiency virus; CHR, C-terminal heptad repeat; NHR, N-terminal heptad repeat; CCF, cell–cell fusion; VCF, virus–cell fusion; 6-HB, six-helix bundle; HP, hydrophobic pocket; EC₅₀, effective concentration for 50% inhibition; TC₅₀, concentration causing 50% cytotoxicity; DMSO, dimethylsulfoxide; DMEM, Dulbecco's modified eagle medium; FBS, fetal bovine serum; SAR, structure–activity relationship; POPC, 1-palmitoyl-2-oleoyl-*sn*-glycero-3-phosphocholine

■ REFERENCES

- (1) Melikyan, G. B.; Markosyan, R. M.; Hemmati, H.; Delmedico, M. K.; Lambert, D. M.; Cohen, F. S. Evidence that the transition of HIV-1 gp41 into a six-helix bundle, not the bundle configuration, induces membrane fusion. *J. Cell Biol.* **2000**, *151*, 413–423. Comment is in *J. Cell Biol.* **2000**, *151* (2), F9–F14.
- (2) Gallo, S. A.; Puri, A.; Blumenthal, R. HIV-1 gp41 six-helix bundle formation occurs rapidly after the engagement of gp120 by CXCR4 in the HIV-1 Env-mediated fusion process. *Biochemistry (Moscow)* **2001**, *40*, 12231–12236.
- (3) Steger, H. K.; Root, M. J. Kinetic dependence to HIV-1 entry inhibition. *J. Biol. Chem.* **2006**, *281*, 25813–25821.
- (4) Eckert, D. M.; Kim, P. S. Mechanisms of viral membrane fusion and its inhibition. *Annu. Rev. Biochem.* **2001**, *70*, 777–810.
- (5) Naider, F.; Anglister, J. Peptides in the treatment of AIDS. *Curr. Opin. Struct. Biol.* **2009**, *19*, 473–482.
- (6) Dimitrov, A. S.; Louis, J. M.; Bewley, C. A.; Clore, G. M.; Blumenthal, R. Conformational changes in HIV-1 gp41 in the course of HIV-1 envelope glycoprotein-mediated fusion and inactivation. *Biochemistry (Moscow)* **2005**, *44*, 12471–12479.
- (7) Eggink, D.; Baldwin, C. E.; Deng, Y.; Langedijk, J. P.; Lu, M.; Sanders, R. W.; Berkhout, B. Selection of T1249-resistant human immunodeficiency virus type 1 variants. *J. Virol.* **2008**, *82*, 6678–6688.
- (8) Greenberg, M. L.; Cammack, N. Resistance to enfuvirtide, the first HIV fusion inhibitor. *J. Antimicrob. Chemother.* **2004**, *54*, 333–340.
- (9) He, Y.; Xiao, Y.; Song, H.; Liang, Q.; Ju, D.; Chen, X.; Lu, H.; Jing, W.; Jiang, S.; Zhang, L. Design and evaluation of sifuvirtide, a novel HIV-1 fusion inhibitor. *J. Biol. Chem.* **2008**, *283*, 11126–11134.
- (10) Louis, J. M.; Bewley, C. A.; Gustchina, E.; Aniana, A.; Clore, G. M. Characterization and HIV-1 fusion inhibitory properties of monoclonal Fabs obtained from a human non-immune phage library selected against diverse epitopes of the ectodomain of HIV-1 gp41. *J. Mol. Biol.* **2005**, *353*, 945–951.
- (11) Welch, B. D.; Francis, J. N.; Redman, J. S.; Paul, S.; Weinstock, M. T.; Reeves, J. D.; Lie, Y. S.; Whitby, F. G.; Eckert, D. M.; Hill, C. P.; Root, M. J.; Kay, M. S. Design of a potent D-peptide HIV-1 entry inhibitor with a strong barrier to resistance. *J. Virol.* **2010**, *84*, 11235–11244.
- (12) Chan, D. C.; Fass, D.; Berger, J. M.; Kim, P. S. Core structure of gp41 from the HIV envelope glycoprotein. *Cell* **1997**, *89*, 263–273.
- (13) Chan, D. C.; Chutkowski, C. T.; Kim, P. S. Evidence that a prominent cavity in the coiled coil of HIV type 1 gp41 is an attractive drug target. *Proc. Natl. Acad. Sci. U.S.A.* **1998**, *95*, 15613–15617.
- (14) Eckert, D. M.; Malashkevich, V. N.; Hong, L. H.; Carr, P. A.; Kim, P. S. Inhibiting HIV-1 entry: discovery of D-peptide inhibitors that target the gp41 coiled-coil pocket. *Cell* **1999**, *99*, 103–115.
- (15) Zhou, G.; Wu, D.; Hermel, E.; Balogh, E.; Gochin, M. Design, synthesis, and evaluation of indole compounds as novel inhibitors targeting Gp41. *Bioorg. Med. Chem. Lett.* **2010**, *20*, 1500–1503.
- (16) Whitby, L. R.; Boyle, K. E.; Cai, L.; Yu, X.; Gochin, M.; Boger, D. L. Discovery of HIV fusion inhibitors targeting gp41 using a

comprehensive alpha-helix mimetic library. *Bioorg. Med. Chem. Lett.* **2012**, *22*, 2861–2865.

(17) Liu, K.; Lu, H.; Hou, L.; Qi, Z.; Teixeira, C.; Barbault, F.; Fan, B. T.; Liu, S.; Jiang, S.; Xie, L. Design, synthesis, and biological evaluation of N-carboxyphenylpyrrole derivatives as potent HIV fusion inhibitors targeting gp41. *J. Med. Chem.* **2008**, *51*, 7843–7854.

(18) Jiang, S.; Tala, S. R.; Lu, H.; Abo-Dya, N. E.; Avan, I.; Gyanda, K.; Lu, L.; Katritzky, A. R.; Debnath, A. K. Design, synthesis, and biological activity of novel 5-((arylfuran-1H-pyrrol-2-yl)methylene)-2-thioxo-3-(3-(trifluoromethyl)phenyl)thiazolidin-4-ones as HIV-1 fusion inhibitors targeting gp41. *J. Med. Chem.* **2011**, *54*, 572–579.

(19) He, X. Y.; Lu, L.; Qiu, J.; Zou, P.; Yu, F.; Jiang, X. K.; Li, L.; Jiang, S.; Liu, S.; Xie, L. Small molecule fusion inhibitors: design, synthesis and biological evaluation of (Z)-3-(5-(3-benzyl-4-oxo-2-thioxothiazolidinylidene)methyl)-N-(3-carboxy-4-hydroxy)phenyl-2,5-dimethylpyrroles and related derivatives targeting HIV-1 gp41. *Bioorg. Med. Chem.* **2013**, *21*, 7539–7548.

(20) Katritzky, A. R.; Tala, S. R.; Lu, H.; Vakulenko, A. V.; Chen, Q. Y.; Sivapackiam, J.; Pandya, K.; Jiang, S.; Debnath, A. K. Design, synthesis, and structure–activity relationship of a novel series of 2-aryl 5-(4-oxo-3-phenethyl-2-thioxothiazolidinylidenemethyl)furan as HIV-1 entry inhibitors. *J. Med. Chem.* **2009**, *52*, 7631–7639.

(21) Sigal, A.; Kim, J. T.; Balazs, A. B.; Dekel, E.; Mayo, A.; Milo, R.; Baltimore, D. Cell-to-cell spread of HIV permits ongoing replication despite antiretroviral therapy. *Nature* **2011**, *477*, 95–98.

(22) Zhou, G.; Wu, D.; Snyder, B.; Ptak, R. G.; Kaur, H.; Gochin, M. Development of indole compounds as small molecule inhibitors of HIV-1 gp41. *J. Med. Chem.* **2011**, *54*, 7220–7231.

(23) Lalezari, J. P.; Eron, J. J.; Carlson, M.; Cohen, C.; DeJesus, E.; Arduino, R. C.; Gallant, J. E.; Volberding, P.; Murphy, R. L.; Valentine, F.; Nelson, E. L.; Sista, P. R.; Dusek, A.; Kilby, J. M. A phase II clinical study of the long-term safety and antiviral activity of enfuvirtide-based antiretroviral therapy. *AIDS* **2003**, *17*, 691–698.

(24) Blangetti, M.; Rosso, H.; Prandi, C.; Deagostino, A.; Venturello, P. Suzuki–Miyaura cross-coupling in acylation reactions, scope and recent developments. *Molecules* **2013**, *18*, 1188–1213.

(25) Miyaura, N.; Suzuki, A. Palladium-catalyzed cross-coupling reactions of organoboron compounds. *Chem. Rev.* **1995**, *95*, 2457–2483.

(26) Akwabi-Ameyaw, A.; Bass, J. Y.; Caldwell, R. D.; Caravella, J. A.; Chen, L.; Creech, K. L.; Deaton, D. N.; Madauss, K. P.; Marr, H. B.; McFadyen, R. B.; Miller, A. B.; Navas, F. 3rd; Parks, D. J.; Spearing, P. K.; Todd, D.; Williams, S. P.; Wisely, G. B. FXR agonist activity of conformationally constrained analogs of GW 4064. *Bioorg. Med. Chem. Lett.* **2009**, *19*, 4733–4739.

(27) Gochin, M.; Cai, L. The role of amphiphilicity and negative charge in glycoprotein 41 interactions in the hydrophobic pocket. *J. Med. Chem.* **2009**, *52*, 4338–4344.

(28) Hawkins, P. C.; Skillman, A. G.; Warren, G. L.; Ellingson, B. A.; Stahl, M. T. Conformer generation with OMEGA: algorithm and validation using high quality structures from the Protein Databank and Cambridge Structural Database. *J. Chem. Inf. Model.* **2010**, *50*, 572–584.

(29) Hawkins, P. C.; Nicholls, A. Conformer generation with OMEGA: learning from the data set and the analysis of failures. *J. Chem. Inf. Model.* **2012**, *52*, 2919–2936.

(30) Katritzky, A. R.; Pilarski, B.; Urogdi, L. Efficient conversion of nitriles to amides with basic hydrogen peroxide in dimethyl sulfoxide. *Synthesis* **1989**, *12*, 949–950.

(31) Hollmann, A.; Matos, P. M.; Augusto, M. T.; Castanho, M. A.; Santos, N. C. Conjugation of cholesterol to HIV-1 fusion inhibitor C34 increases peptide–membrane interactions potentiating its action. *PLoS One* **2013**, *8*, e60302.

(32) Jiang, S.; Debnath, A. K. A salt bridge between an N-terminal coiled coil of gp41 and an antiviral agent targeted to the gp41 core is important for anti-HIV-1 activity. *Biochem. Biophys. Res. Commun.* **2000**, *270*, 153–157.

(33) He, Y.; Liu, S.; Jing, W.; Lu, H.; Cai, D.; Chin, D. J.; Debnath, A. K.; Kirchhoff, F.; Jiang, S. Conserved residue Lys574 in the cavity of

HIV-1 Gp41 coiled-coil domain is critical for six-helix bundle stability and virus entry. *J. Biol. Chem.* **2007**, *282*, 25631–25639.

(34) Gochin, M.; Whitby, L. R.; Phillips, A. H.; Boger, D. L. NMR-assisted computational studies of peptidomimetic inhibitors bound in the hydrophobic pocket of HIV-1 glycoprotein 41. *J. Comput.-Aided Mol. Des.* **2013**, *27*, 569–582.

(35) Allen, W. J.; Rizzo, R. C. Computer-aided approaches for targeting HIVgp41. *Biology* **2012**, *1*, 311–338.

(36) Sabin, C.; Corti, D.; Buzon, V.; Seaman, M. S.; Lutje Hulsik, D.; Hinz, A.; Vanzetta, F.; Agatic, G.; Silacci, C.; Mainetti, L.; Scarlatti, G.; Sallusto, F.; Weiss, R.; Lanzavecchia, A.; Weissenhorn, W. Crystal structure and size-dependent neutralization properties of HK20, a human monoclonal antibody binding to the highly conserved heptad repeat 1 of gp41. *PLoS Pathog.* **2010**, *6*, e1001195.

(37) Eldridge, M. D.; Murray, C. W.; Auton, T. R.; Paolini, G. V.; Mee, R. P. Empirical scoring functions: I. The development of a fast empirical scoring function to estimate the binding affinity of ligands in receptor complexes. *J. Comput.-Aided Mol. Des.* **1997**, *11*, 425–445.

(38) Cai, L.; Gochin, M. A novel fluorescence intensity screening assay identifies new low molecular weight inhibitors of the gp41 coiled coil domain of HIV-1. *Antimicrob. Agents Chemother.* **2007**, *51*, 2388–2395.

(39) Gochin, M. A suite of modular fluorescence assays interrogate the human immunodeficiency virus glycoprotein-41 coiled coil and assist in determining binding mechanism of low molecular weight fusion inhibitors. *Assay Drug Dev. Technol.* **2012**, *10*, 407–416.

(40) Platt, E. J.; Wehrly, K.; Kuhmann, S. E.; Chesebro, B.; Kabat, D. Effects of CCR5 and CD4 cell surface concentrations on infections by macrophagetropic isolates of human immunodeficiency virus type 1. *J. Virol.* **1998**, *72*, 2855–2864.

(41) Wei, X.; Decker, J. M.; Liu, H.; Zhang, Z.; Arani, R. B.; Kilby, J. M.; Saag, M. S.; Wu, X.; Shaw, G. M.; Kappes, J. C. Emergence of resistant human immunodeficiency virus type 1 in patients receiving fusion inhibitor (T-20) monotherapy. *Antimicrob. Agents Chemother.* **2002**, *46*, 1896–1905.

(42) Ciminale, V.; Felber, B. K.; Campbell, M.; Pavlakis, G. N. A bioassay for HIV-1 based on Env-CD4 interaction. *AIDS Res. Hum. Retroviruses* **1990**, *6*, 1281–1287.

(43) Lackman-Smith, C.; Osterling, C.; Luckenbaugh, K.; Mankowski, M.; Snyder, B.; Lewis, G.; Paull, J.; Profy, A.; Ptak, R. G.; Buckheit, R. W., Jr.; Watson, K. M.; Cummins, J. E., Jr.; Sanders-Beer, B. E. Development of a comprehensive human immunodeficiency virus type 1 screening algorithm for discovery and preclinical testing of topical microbicides. *Antimicrob. Agents Chemother.* **2008**, *52*, 1768–1781.

(44) Kagiampakis, I.; Gharibi, A.; Mankowski, M. K.; Snyder, B. A.; Ptak, R. G.; Alatas, K.; LiWang, P. J. Potent strategy to inhibit HIV-1 by binding both gp120 and gp41. *Antimicrob. Agents Chemother.* **2011**, *55*, 264–275.

(45) Popovic, M.; Read-Connole, E.; Gallo, R. C. T4 positive human neoplastic cell lines susceptible to and permissive for HTLV-III. *Lancet* **1984**, *2*, 1472–1473.

(46) Popovic, M. S.; Gartner, E.; Read-Connole, B.; Beaver, M.; Reitz, M. Cell tropism and expression of HIV-1 isolated in natural targets. In *Retroviruses of Human A.I.D.S. and Related Animal Diseases*; Valette, L., Girard, M., Eds.; Pasteur Vaccins: Marnes-La-Coquette, France, 1989; pp 219–224.

(47) Chackerian, B.; Long, E. M.; Luciw, P. A.; Overbaugh, J. Human immunodeficiency virus type 1 coreceptors participate in postentry stages in the virus replication cycle and function in simian immunodeficiency virus infection. *J. Virol.* **1997**, *71*, 3932–3939.

(48) Ratner, L.; Haseltine, W.; Patarca, R.; Livak, K. J.; Starcich, B.; Josephs, S. F.; Doran, E. R.; Rafalski, J. A.; Whitehorn, E. A.; Baumeister, K.; et al. Complete nucleotide sequence of the AIDS virus, HTLV-III. *Nature* **1985**, *313*, 277–284.

(49) Ptak, R. G.; Gallay, P. A.; Jochmans, D.; Halestrap, A. P.; Ruegg, U. T.; Pallansch, L. A.; Bobardt, M. D.; de Bethune, M. P.; Neyts, J.; De Clercq, E.; Dumont, J. M.; Scalfaro, P.; Besseghir, K.; Wenger, R. M.; Rosenwirth, B. Inhibition of human immunodeficiency virus type 1 replication in human cells by Debio-025, a novel cyclophilin binding agent. *Antimicrob. Agents Chemother.* **2008**, *52*, 1302–1317.

(50) Buckheit, R. W., Jr.; Swanstrom, R. Characterization of an HIV-1 isolate displaying an apparent absence of virion-associated reverse transcriptase activity. *AIDS Res. Hum. Retroviruses* **1991**, *7*, 295–302.

(51) Gao, F.; Yue, L.; Craig, S.; Thornton, C. L.; Robertson, D. L.; McCutchan, F. E.; Bradac, J. A.; Sharp, P. M.; Hahn, B. H. Genetic variation of HIV type 1 in four World Health Organization-sponsored vaccine evaluation sites: generation of functional envelope (glycoprotein 160) clones representative of sequence subtypes A, B, C, and E. WHO Network for HIV Isolation and Characterization. *AIDS Res. Hum. Retroviruses* **1994**, *10*, 1359–1368.

(52) Brown, B. K.; Darden, J. M.; Tovanabutra, S.; Oblander, T.; Frost, J.; Sanders-Buell, E.; de Souza, M. S.; Birx, D. L.; McCutchan, F. E.; Polonis, V. R. Biologic and genetic characterization of a panel of 60 human immunodeficiency virus type 1 isolates, representing clades A, B, C, D, CRF01_AE, and CRF02_AG, for the development and assessment of candidate vaccines. *J. Virol.* **2005**, *79*, 6089–6101.

(53) Jagodzinski, L. L.; Wiggins, D. L.; McManis, J. L.; Emery, S.; Overbaugh, J.; Robb, M.; Bodrug, S.; Michael, N. L. Use of calibrated viral load standards for group M subtypes of human immunodeficiency virus type 1 to assess the performance of viral RNA quantitation tests. *J. Clin. Microbiol.* **2000**, *38*, 1247–1249.

(54) Grant, J. A.; Gallardo, M. A.; Pickup, B. T. A fast method of molecular shape comparison: a simple application of a Gaussian description of molecular shape. *J. Comput. Chem.* **1996**, *17*, 1653–1666.

(55) Nicholls, A.; McGaughey, G. B.; Sheridan, R. P.; Good, A. C.; Warren, G.; Mathieu, M.; Muchmore, S. W.; Brown, S. P.; Grant, J. A.; Haigh, J. A.; Nevins, N.; Jain, A. N.; Kelley, B. Molecular shape and medicinal chemistry: a perspective. *J. Med. Chem.* **2010**, *53*, 3862–3886.

(56) McGann, M. FRED pose prediction and virtual screening accuracy. *J. Chem. Inf. Model.* **2011**, *51*, 578–596.